Interface reactions and Kirkendall voids in metal organic vapor-phase epitaxy grown $Cu(In,Ga)Se_2$ thin films on GaAs

C. H. Lei, A. A. Rockett,[a] and I. M. Robertson
Department of Materials Science and Engineering, University of Illinois at Urbana-Champaign, 1304 W. Green Street, Urbana, Illinois 61801

N. Papathanasiou and S. Siebentritt
Hahn-Meitner Institut, Glienicker Straße 100, D-14109 Berlin, Germany

(Received 19 June 2006; accepted 19 September 2006; published online 14 December 2006)

$Cu(In_{1-x}Ga_x)Se_2$ (CIGS) films were grown on (001) GaAs at 570 or 500 °C by means of metal organic vapor-phase epitaxy. All films were Cu-rich [Cu/(In+Ga)>1] with pseudomorphic Cu_2Se second phase particles found only on the growth surface. During growth, diffusion of Ga from the substrate and vacancies generated by the formation of CIGS from Cu_2Se at the surface occurred. The diffusion processes lead to the formation of Kirkendall voids at the GaAs/CIGS interface. Transmission electron microscopy and nanoprobe energy dispersive spectroscopy were used to analyze the diffusion and void formation processes. The diffusivity of Ga in CIGS was found to be relatively low. This is postulated to be due to a comparatively low concentration of point defects in the epitaxial films. A reaction model explaining the observed profiles and voids is proposed. © *2006 American Institute of Physics*. [DOI: 10.1063/1.2397282]

I. INTRODUCTION

Photovoltaic materials are receiving significant attention because of increasing concerns about existing energy resource lifetimes and the need for distributed power generation. Photovoltaics based on $Cu(In_{1-x}Ga_x)Se_2$ (CIGS) alloys with $x<0.3$ have the highest performance of any thin film solar cells and show excellent long-term stability.[1,2] Although progress has been made in improving the performance of CIGS solar cell devices, a fundamental understanding of the mechanisms limiting the overall efficiency is still lacking. To achieve lower costs and higher efficiencies, it will be necessary to develop devices based on wider-gap absorber layers ($x>0.3$) and tandem-junction devices. Unfortunately, these devices show a significant loss of efficiency relative to the lower Ga-content films.[2–4] Doping in these materials is due to intrinsic defects such as vacancies, interstitials, and antisites, which thus play a major role in junction formation in these solar cells. To study these defects, epitaxial films were grown, since epitaxial layers without grain boundaries are more easily characterized both optoelectronically and structurally than are polycrystalline materials.

Epitaxial CIGS films have been grown on GaAs with both polar (111) surface orientations, as well as on (001) Si (Ref. 5) and other substrates by means of molecular beam epitaxy (MBE),[5,6] sputtering,[7–9] and metalorganic vapor-phase epitaxy (MOVPE).[10,11] Studies of the efficiencies of resulting solar cells, photoluminescence, surface morphology, growth mechanisms, and microstructure of the epitaxial films have been reported [cf. Refs. 5–14]. MOVPE, in particular, is well known for large-area growth of high-quality epitaxial films on large substrates[15,16] and is therefore of special interest among these techniques.

In this paper, results on the nanostructure and nanochemistry of epitaxial CIGS grown by MOVPE on GaAs (001) substrates are reported. Films were characterized by transmission electron microscopy (TEM) and energy-dispersive x-ray spectroscopy (EDS). The combination of techniques allows us to examine the local composition and structure of films in probed areas of <2 nm diameter.

II. EXPERIMENTAL PROCEDURE

Epitaxial CIGS thin films were grown in an Aixtron AIX200 MOVPE reactor on "epiready" (001)GaAs wafers. Trimethyl indium, ditertiary butyl selenide and cyclopentadienyl copper triethyl phosphine, and triethyl gallium were used as In, Se, Cu, and Ga precursors, respectively. The standard processing time was 4 h, and the pressure was kept at 50 mbar in the reactor. Films with various Ga/(In+Ga) ratios were grown at 570 or 500 °C in order to understand the effects of growth temperature and composition. All films were copper rich and showed Cu_2Se second phases on the surfaces. Final film thicknesses were 0.2–0.4 μm, corresponding to a growth rate of 0.05–0.1 μm/h, with the growth rate limited primarily by the Cu precursor.[11]

Standard TEM sample preparation procedures, wire sawing, gluing, grinding, and Ar ion milling, were applied to prepare cross-sectional and plan-view TEM samples. To minimize the introduction of artifacts such as Cu contamination or In island formation on the surfaces during ion milling the samples were mounted on Ni sample holder rings, cooled with liquid nitrogen, and ion milling was carried out at shallow ion incidence angles.[17,18] No evidence of sample-preparation-related artifacts was found in any of the measurements including no evidence of In islands either in images or in the nano-EDS measurements. The samples were examined shortly after preparation, as there was evidence for a gradual deterioration in air, primarily due to surface oxida-

[a]Electronic mail: arockett@uiuc.edu

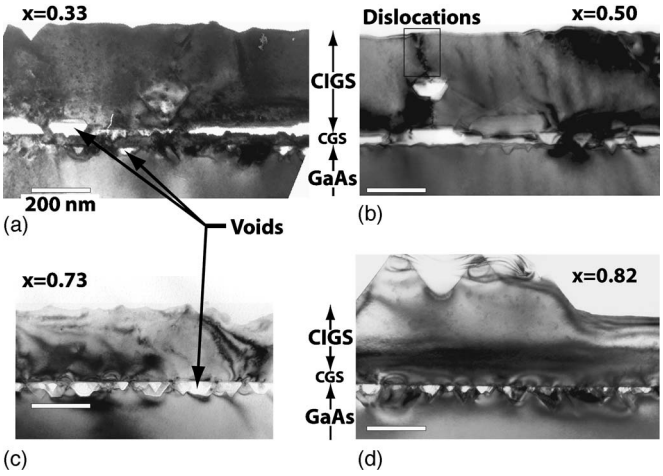

FIG. 1. Electron micrographs show the cross-sectional images of four Cu(InGa)Se_2 (CIGS) films grown at 570 °C with compositions x=Ga/(In+Ga) for (a) x=0.33, (b) x=0.5, (c) x=0.73, and (d) x=0.82. All images are the same scale with 200 nm scale marks on each. Several examples of Kirkendal voids are marked and others are visible including one in the x=0.5 film that appears to be associated with a dislocation tangle (marked with a box).

tion. The microstructure of the films was observed in a Philips CM 12 TEM, while the EDS composition measurements were performed in a VG HB501 dedicated scanning TEM (STEM) with a beam diameter of ~1.3 nm. Effective probed volumes were less than 2 nm in diameter within the electron-transparent volume. Additional measurements were performed in a JEOL 2010 F field-emission gun STEM with an effective 1 nm probe size.

EDS analyses were quantified using standard EDS data analysis software. Because of the thickness of the TEM specimens (15–100 nm, but typically 60±20 nm), no correction for absorption or fluorescence was applied to the data. Elemental sensitivity factors were determined with reference to a variety of standard materials. Manual fits to some of the EDS spectra using Gaussian peaks were also performed to check the automated fitting algorithm and good agreement was obtained. Counting times were adjusted to minimize scatter in the data but were generally kept to a minimum to avoid the risk of electron beam damage to the samples. Typically the precision of compositions is ±1.5 at. % and the accuracy is better than ±0.8 at. % in any element under the normal analysis conditions. These were determined from the scatter in the CIGS compositions as a function of counting time and composition measurements of GaAs samples, which have a Ga:As atom ratio of exactly 1.00.[19]

III. RESULTS

A. Films grown at 570 °C

In Fig. 1, cross-sectional micrographs from four films with varying Ga/(In+Ga) ratios, and which were grown at 570 °C, are compared. Note that some surface roughness occurs on the as grown samples, especially those with high Ga contents. Based on both electron diffraction patterns and lattice images, all films were found to be epitaxial on the (001) GaAs substrates. Diffraction patterns reveal that all films are single-domain (001) oriented, with the c axis of the

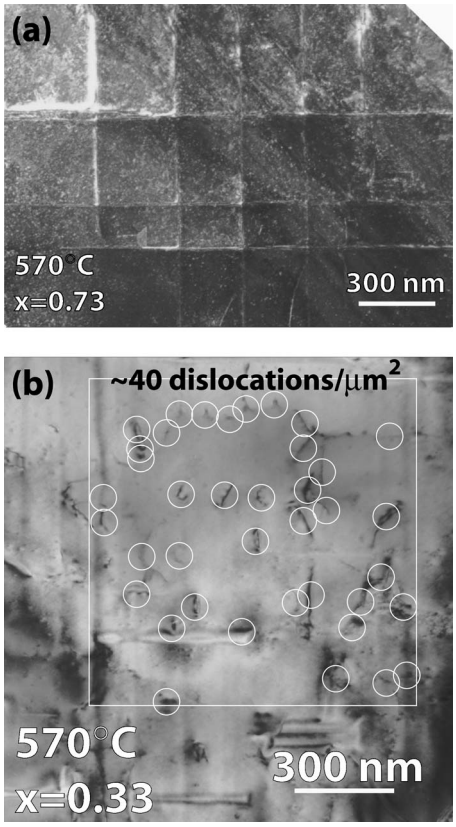

FIG. 2. (a) A plan-view electron micrograph of the sample grown at 570 °C with x=0.73 showing the misfit dislocation network (horizontal and vertical lines) accommodating the lattice misfit strain. The dislocation spacing is approximately 300 nm on average, although this layer shows some that are smaller. No threading dislocations are visible in this image. (b) Threading dislocations in a film, marked with circles.

chalcopyrite unit cell along the film normal. The threading dislocation density was ~109 cm^{-2}. Interfacial misfit dislocations, such as shown in Fig. 2, were observed where the film and substrate were in direct contact. The approximate average misfit dislocation spacings were 100, 150, and 300 nm for the x=0.33, 0.50, and 0.73 films, respectively. Other defects such as stacking faults and twins were found occasionally.

All 570 °C films examined show tetrahedral voids near the GaAs/CIGS interface, but always on the GaAs side. Each void had a triangular cross section as seen in the cross-sectional images in Fig. 1. The orientation of the triangle was inverted when samples prepared from the same specimen were sliced perpendicular to each other along ⟨110⟩ substrate directions. Viewed in plan view through the interface they were rectangular. There was no correlation of the size of the voids and the film composition. The voids in the GaAs exhibit facets on the {111} planes.

Large tetrahedral voids were found within the CIGS layer for the films with x=Ga/(In+Ga)≤0.50, as shown in Fig. 1(c) and 1(d). These voids are bigger than those in the GaAs, are separated from the interface by a layer of altered composition (see below), and can be connected to each other to form hollow pipes. Facets of these voids consist of {112} close-packed planes of the tetrahedral unit cell; these planes are equivalent to the {111} planes of a zinc blende lattice.

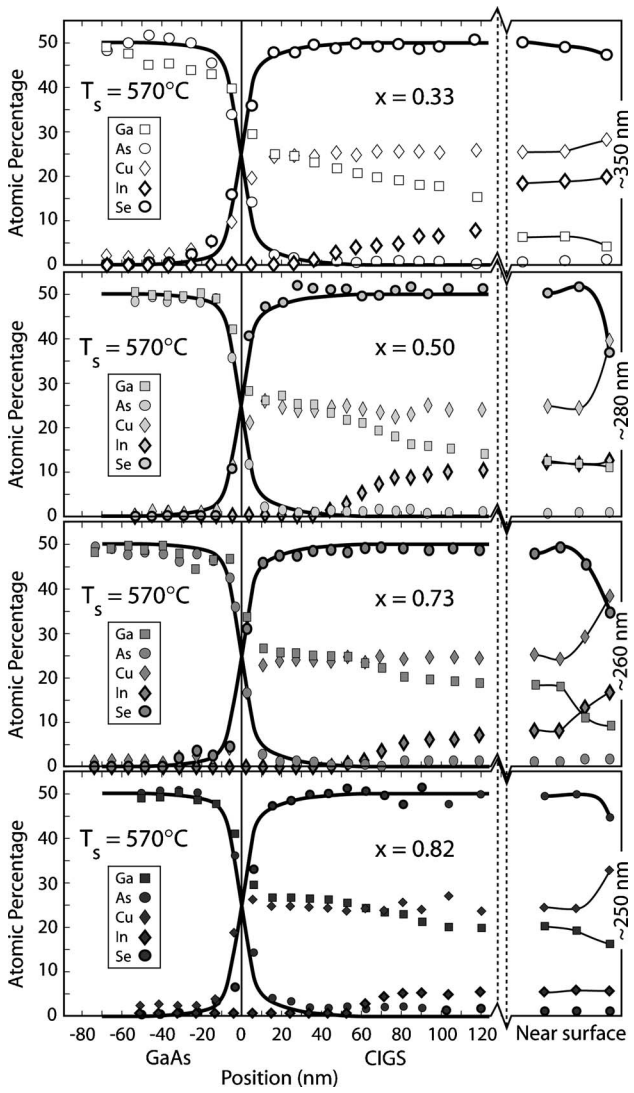

FIG. 3. A montage of profiles for the 570 °C samples in Fig. 1, showing the change in atomic concentrations across the CIGS/GaAs interface region. Several data points near the surface are also included. The horizontal scale is the same for these points and the surface position is shown for each film. The width of the CIGS/GaAs interface is ~40 nm although the interface in images was atomically abrupt. The breadth of the observed interface is due to interfacial roughness through the probed volume.

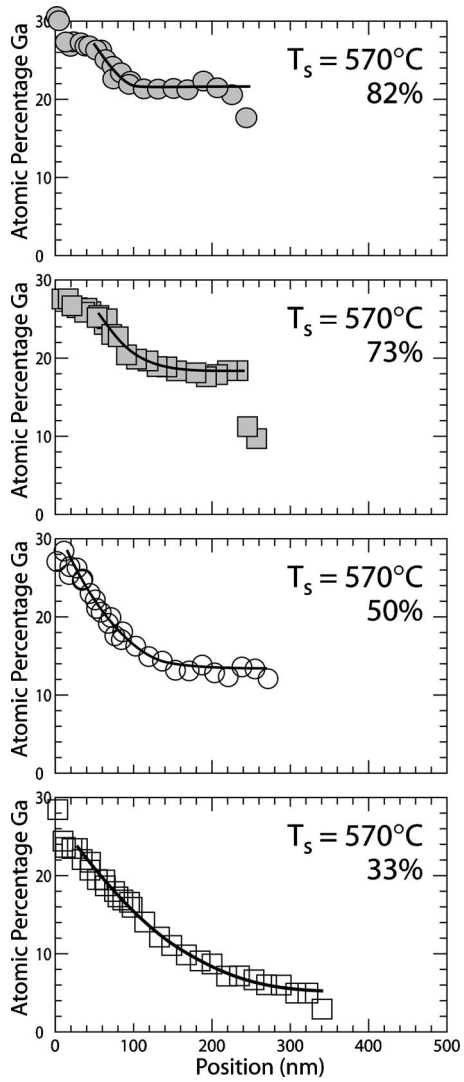

FIG. 4. Shows the Ga concentration across the four films with different x values and error-function curves fit to the data and from which the Ga diffusivities were extracted.

The voids do not penetrate to the film surface, but rather are sealed within the film. In the film with a nominal 50% Ga/In+Ga ratio, [Fig. 1(b)], a relatively large void was found roughly in the middle of the film in association with a tangle of dislocations.

Elemental depth profiles for the films presented in Fig. 1 are shown in Fig. 3. The changes in Cu and Se profiles were found to be small from the top to the bottom of the films, excluding the surface itself where Cu_ySe was observed ($y \sim 2$). Although the observed compositional variations are close to the noise level in the EDS analysis, they are probably real and related to variations in the point defect density. The point defect density could not be established as no additional diffraction features commensurate with defect ordering were observed. [20,21]

The sum of the In and Ga concentrations is roughly constant throughout the film, although substantial variations in Ga and In were found through the depth of the films. The variation in Ga concentration throughout the film is shown in Fig. 4. The Ga concentration drops from ~26±1 at. % in the interfacial CGS layer to a level that increases with increasing x. This observation is consistent with Ga diffusion out of the substrates. No In was detected at the CIGS/GaAs interface in any film grown at 570 °C. In other words, a pure $CuGaSe_2$ (CGS, $x=1$) layer occurs at this interface. The thickness of the CGS layer varies from ~15 nm for $x=0.33$ and 0.50 to ~50 nm for $x=0.73$ and 0.82. The width of the CIGS/GaAs interface is ~40 nm. This width results from interface roughness through the measured volume rather than interdiffusion as the width is independent of growth time and, as shown below, growth temperature. Presumably As diffuses rapidly in the CIGS as it is not observed in excess even though Ga is found to be released into the CIGS. Secondary ion mass spectrometry showed no As in the bulk of the CIGS layer, confirming the EDS results.

The surface of the films was found to be Cu rich as grown, which was expected based on the Cu-rich overall composition of the films. EDS analysis of the 2 nm thick

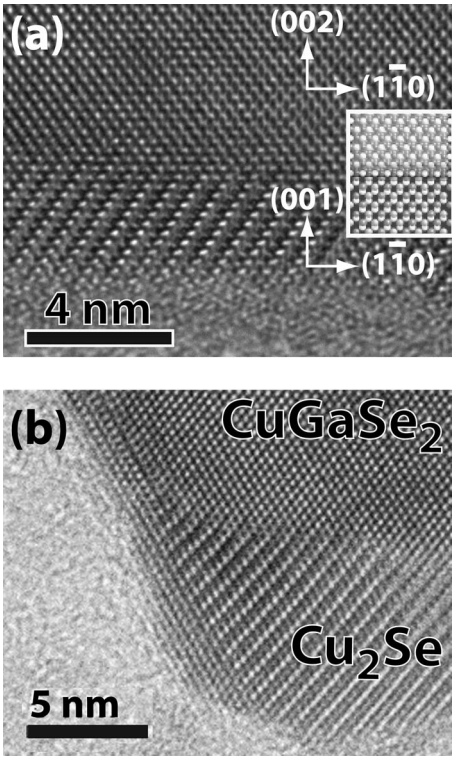

FIG. 5. Cross sectional TEM lattice images of the surface of a CIGS film grown at 570 °C showing the presence of a Cu_2Se layer. The zone axis of the images is [110]. The composition of the layer was confirmed by EDS. (a) Indicates the crystallographic indexing of the $CuGaSe_2$ and Cu_2Se regions and an inset showing a simulation of the two lattices. (b) Shows a thicker Cu_2Se region on the surface in one region.

surface layer indicates that the compound is Cu_2Se. Two TEM lattice images in which this surface layer is visible are presented in Fig. 5. The Cu_2Se grows epitaxially on the $CuGaSe_2$ with two of the cube axes of the Cu_2Se parallel to the basal plane of the CGS unit cell yielding a structure as shown in the inset in Fig. 5. There is a twist of the lattice planes in the Cu_2Se (they do not continue the substrate planes in a straight line) that may be due to the Poisson effect and lattice misfit strain accommodation. The Cu_2Se was not single crystalline but was comprised of small grains, with some having a size between 10 and 20 nm. The misorientation between these grains was small.

B. films grown at 500 °C

The films grown at 500 °C (see Fig. 6), show similarities and differences to the films grown at the higher temperature. The threading dislocation density was the same, 10^9 cm^{-2}, and the misfit dislocation spacing was ~100 and ~215 nm for the $x=0.10$ and 0.33 films, respectively. Voids at the GaAs/CIGS interface were in the GaAs, although the voids dimension smaller, $<\sim 10$ nm, than in the films grown at 570 °C. Again, there was no correlation of void size with composition. The most striking difference between the films grown at different temperatures is that at the lower temperature no large voids occur in the CIGS, even for the lowest Ga-content film ($x=0.10$) and, as shown below, no pure CGS layer occurs at this interface. In contrast to the higher-temperature growths, all voids occurred at the heterointerface. Occasionally small, ~10 nm, Cu-rich particles (probably copper arsenides) were found in the interfacial areas.

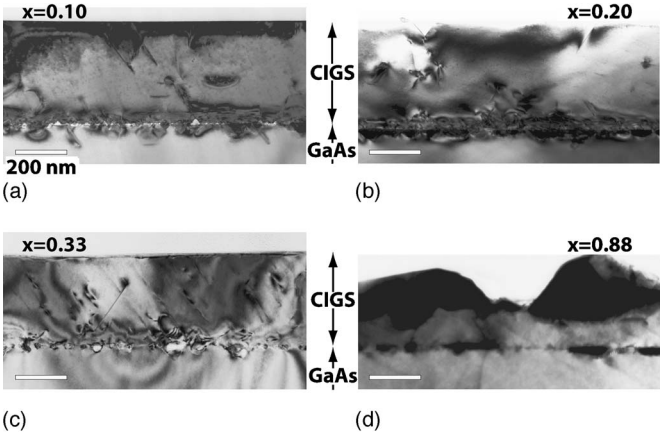

FIG. 6. Cross-sectional images of four CIGS films grown at 500 °C with x values as marked; (a) $x=0.1$, (b) $x=0.2$, (c) x=0.33, and (d) $x=0.88$. All images are the same scale with 200 nm scale marks on each image.

Elemental depth profiles near the heterojunction of the four 500 °C films as well as the near-surface behavior are presented in Fig. 7. Similar to the 570 °C films, no systematic change was found for the Se and Cu compositions across the depth of the films. However, a close inspection of the Cu profiles indicates one analysis point near the interface where the Cu appears to penetrate beyond the other CIGS constituents in the low-Ga samples ($x=0.1$, 0.2, and 0.33). Furthermore, the As signal in these measurements is anomalously high compared to the Ga signal in the GaAs near the interface. These anomalous points are marked with arrows in the figure and confirm the formation of copper arsenides in a very thin layer (~5 nm) near the interface.

The EDS measurements show no pure $CuGaSe_2$ layer, consistent with the microstructural observations (Fig. 5). The surface of the films was Cu rich as expected based on the growth conditions, but the Cu-rich region was less than 10 nm thick, which is significantly thinner than that of the 570 °C samples. Although no pure CGS layer was found at the interface, the Ga profiles shown in Fig. 8 indicate a graded $x=Ga/In+Ga$ region, with x rising to a value near unity at the heterojunction. Based on these results it is proposed that the formation of a CGS layer is a prerequisite for formation of internal voids.

IV. DISCUSSION

The most significant observations in the results are as follows (1) Voids are observed in the GaAs side of the CIGS/GaAs interface in all films irrespective of the growth temperature. (2) A CGS layer is found between the CIGS and the GaAs in the films grown at 570 °C, but not at 500 °C. (3) Voids are found in the CIGS layer at the interface between the CGS and CIGS layers; this occurs in films grown at 570 °C only. (4) The surface of all films is covered by Cu_2Se. (5) A Cu-rich layer at the CIGS/GaAs interface, probably in the form of an arsenide, exists in films grown at 500 °C only.

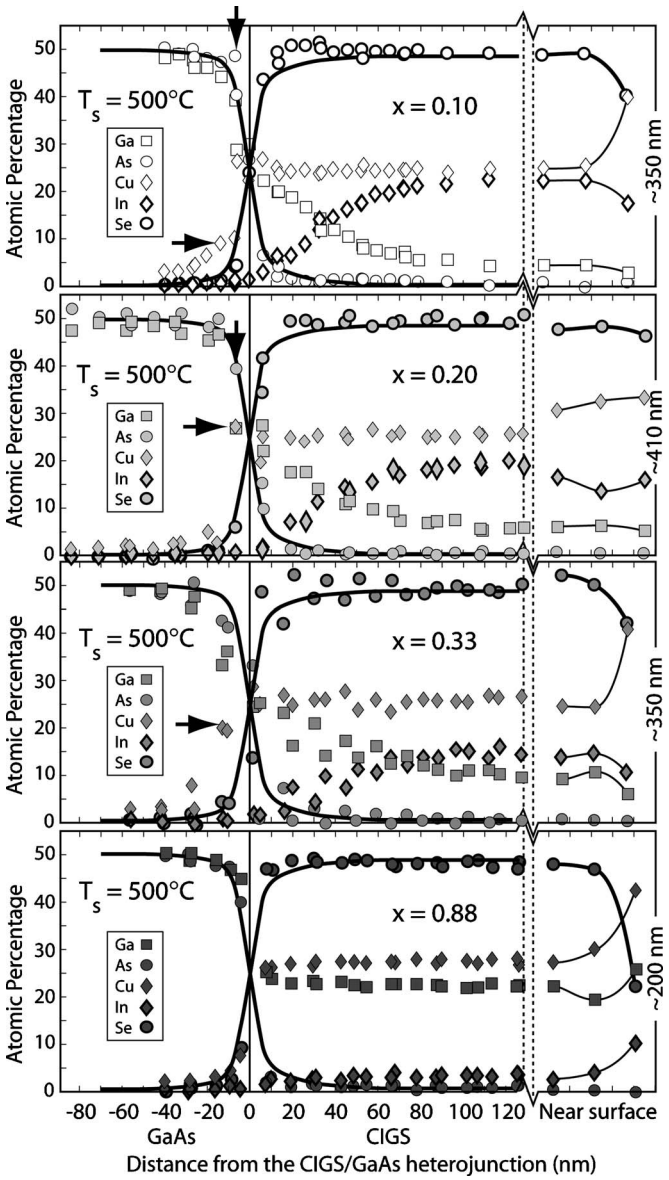

FIG. 7. Quantitative μ-EDS composition of four CIGS films grown at 500 °C near the heterojunction. Data for both the coarse and fine EDS profiles are included. Arrows indicate the presence of an As and Cu rich region near the heteroepitaxial interface. Several data points near the surface of the films are included. The horizontal scale is the same as for the rest of the film and the film thickness is given for each. Note that the outermost data points generally are not fully within the Cu_2Se layer, as evidenced by the composition and residual group III elemental signals.

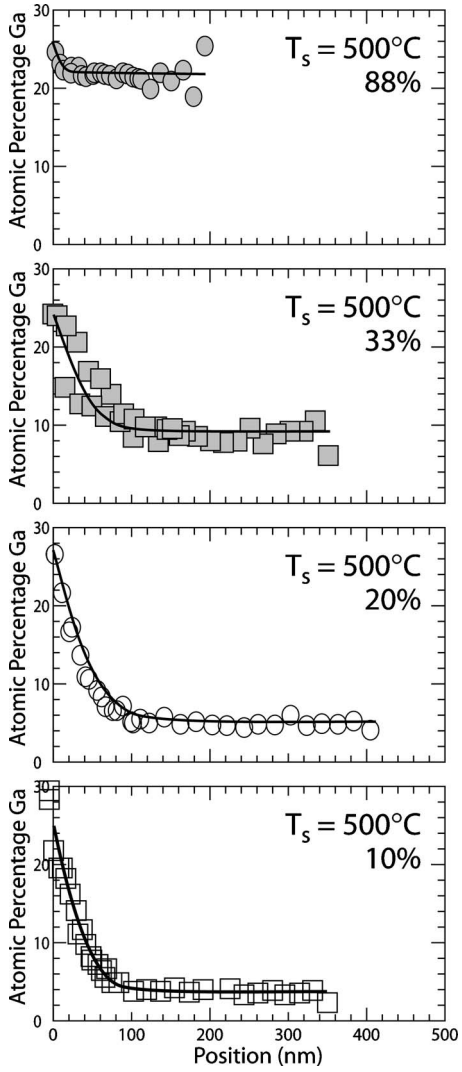

FIG. 8. Shows the Ga concentration across the four films with different x values and error-function curves fit to the data and from which the Ga diffusivities were extracted.

Voids on the GaAs side of the CIGS/GaAs interface formed at both growth temperatures, whereas at 570 °C, voids were found in films with $x<0.5$ at the interface between the CGS and the CIGS. Both types of voids are consistent with their being Kirkendall voids rather than growth defects. In other words, they are the result of coalescence of vacancies moving counter to an outward atomic flux through the CIGS from the GaAs. The moving species are Ga and As in this case. The voids are tetrahedral with {111} facets. This was determined by indexing the crystal and by comparison to the overlying epitaxial layer. It is surprising that the {111} facets form because {110} planes of GaAs are more stable than {111} planes. However, for the surface orientation given (110) and $(1\bar{1}0)$ planes are normal to the (001) plane. Consequently they do not form simple voids. Furthermore, the void facets are not free surfaces and may be covered by a surfactant layer derived from the $CuGaSe_2$ (for example, a coating of Se atoms), which could reduce the energy of the {111} surfaces dramatically. The activity of As in the void is presumably also much higher than it would be on a free surface. It seems likely that the choice of {111} planes is the result of a combination of effects including the amount of surface needed to form a closed void and the chemistry of those surfaces within the voids.

To determine the diffusion kinetics active during MOVPE the Ga diffusion profiles shown in Fig. 4 and 8 were fit using error functions, which are characteristic of diffusion from a fixed-concentration source. The error function behavior shows that the Ga profile is determined by a simple diffusion-limited mechanism rather than by the kinetics of decomposition of the GaAs.

Diffusion coefficients were extracted from the fits as a function of growth temperature and Ga/(In+Ga) ratio. The resulting values are given in Table I and are plotted in Fig. 9. Diffusivities fit for low-Ga content films are accurate to

TABLE I. Diffusion coefficients for Ga in CIGS.

Ga/In+Ga ratio	0.10	0.20	0.33	0.50	0.73	0.82	0.88
T_s=570 °C							
Diffusivity ($cm^2\ s^{-1}$)			1×10^{-14}	3×10^{-15}	1×10^{-15}	4×10^{-16}	
Misfit spacing (nm)			100	150	300		
T_s=500 °C							
Diffusivity ($cm^2\ s^{-1}$)	1×10^{-15}	8×10^{-16}	8×10^{-16}				6×10^{-17}
Misfit spacing (nm)	100		215				

±30% or better while the fits for higher Ga contents are less reliable. Approximate error bars are indicated in Fig. 9. The fits for the 570 °C film results are more reliable than those for the 500 °C films, especially in the presence of high Ga concentrations where only a few data points show the diffusion behavior. The results suggest that the Ga diffusivity decreases with increasing Ga content in the high-temperature film but that the composition dependence is much smaller at lower temperatures, suggesting that a different diffusion mechanism may become active. A reduction in diffusion rate in CIGS for group III elements with increasing Ga content is consistent with other studies of this material. The diffusivities are approximately three orders of magnitude smaller than previously obtained values for both single-crystal[9] and polycrystalline[22,23] films (see the comparison in Fig. 9). In previous studies the diffusivity data suggest a very low activation energy of ~0.5 eV. The activation energy for diffusion in the current study is higher, roughly 1 eV. Grain boundary diffusion often has a low activation energy but is not consistent with the Ga distributions observed, which are similar in grains and grain boundaries, indicating uniform diffusion in polycrystals, such as were studied by others. Furthermore, grain boundary diffusion is not possible in single crystals such as the epitaxial growth results discussed here and in Schroeder *et al.*[9]

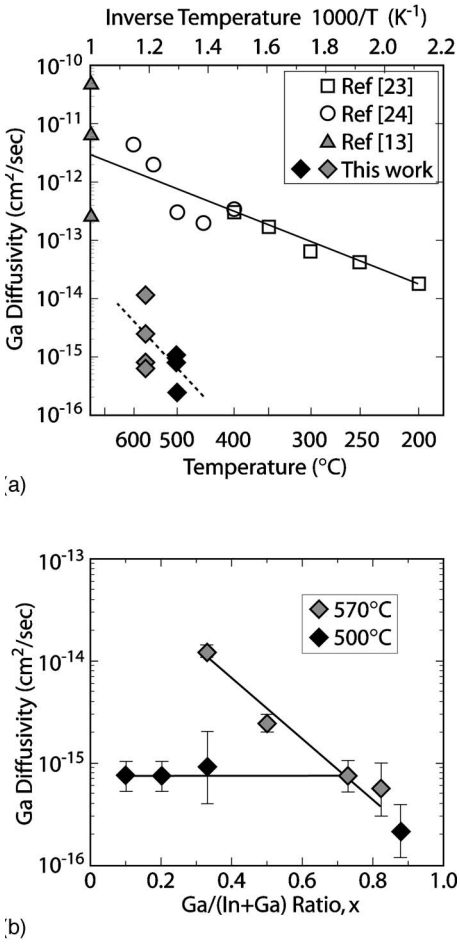

FIG. 9. Plots as a function of deposition temperature (a) and composition (b) for the diffusivities measured here. Experimental values from other studies are shown in (a) for comparison. The potential temperature dependence of bulk diffusion in the epitaxial materials is suggested by the dashed line. Data on epitaxial materials are filled data points.

A possible explanation for the difference in the diffusivities is the concentration of point defects. The films used in this study were grown slowly, requiring about 4 h, and in a Cu-rich environment. Both conditions will result in a relatively low density of point defects. In contrast, the films used in other studies were grown at higher rates, the hybrid sputtering method resulted in energetic particle bombardment of the surface, and the environment was Cu deficient. All these factors combine to result in a film with a higher density of point defects. Support for this difference in the density of point defects comes from photoluminescence linewidths, which are sharper in Cu-rich materials than in group III rich ones. Therefore, the higher diffusivities reported in the literature are attributed to the presence of higher concentrations of point defects. Note that the low defect density does not appear to correlate with improved device results in the MOVPE solar cells.

Based on the microstructural and microchemical observations the following growth model is proposed; the atomic transport processes and reactions are shown schematically in Fig. 10. Cu and Se arriving at the growth surface contribute to the formation of the Cu_2Se layer, while In and Ga dissolve in this layer and precipitate out as nearly stoichiometric CIGS at the CIGS/Cu_2Se interface. Additional growth occurs by group III elements diffusing outward from the substrate. However, because substrate Ga does not pass through the entire film, the moving species must be vacancies rather than group III atoms. Thus, the group III element at the CIGS surface reacts with the Cu_2Se, resulting in a vacancy on the group III sublattice V_{III}, which diffuses to the GaAs, releasing Ga and As into the CIGS. Transport of the released As through the CIGS probably requires an anion vacancy (V_{Se}) in the CIGS unless the As moves by an interstitial mechanism. Because As is valence 3 and Se is valence 2,

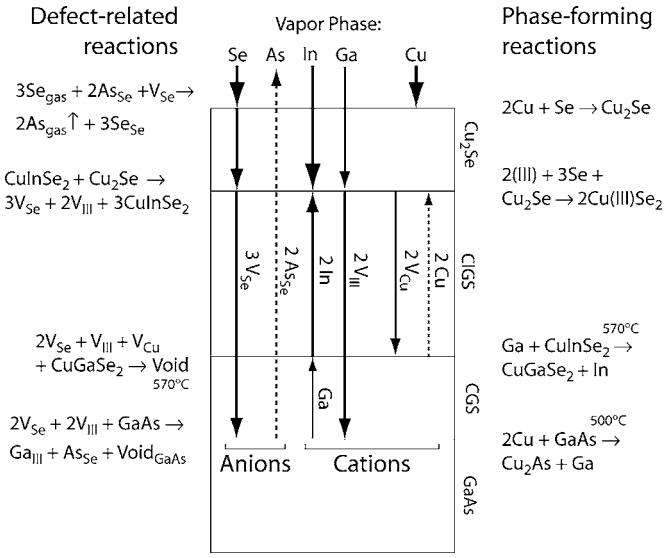

FIG. 10. A schematic of the possible processes occurring in the film at the two temperatures studied. Defect-related reactions are responsible for the Kirkendal voids at the CGS/CIGS and CGS/GaAs interfaces.

three Se vacancies must participate in the diffusion for every two As atoms that move. This will result in excess V_{Se} defects in the CIGS. These do not need to diffuse to any specific location, they merely occur when As atoms replace Se atoms or net *p*-type doping must result from uncompensated As_{Se} defects. The total amount of As in the film is low so that the number of excess vacancies would be negligible. It is also possible that the As substitution could be compensated by changing the valence of Cu from one to two or that an actual increase in *p*-type doping could occur. The As concentration as measured by secondary-ion-mass spectroscopy (SIMS) is too small to cause significant doping. The inward movement of V_{III} and V_{Se} defects is concluded to be responsible for the formation of Kirkendall voids in the substrate.

Between the interfacial voids there is an abrupt junction between the CIGS or CGS and the GaAs substrate. Because this is a lattice mismatched system one would expect to find misfit dislocations at the heterojunction, as shown in Fig. 2. The dislocation spacing is relatively large for the possible misfit magnitudes one might expect. Quantitative estimates are not meaningful given the complexity of the films. The relatively constant density of threading dislocations in the films is presumably the result of growth accidents rather than residual defects due to formation of misfit dislocations. Nonetheless, the dislocation density in most films is considerably higher than the grain boundary density in polycrystalline films. If dislocations are detrimental to solar cell performance, then the higher density in the epitaxial layers could be consistent with the lower device performances.[24,25]

V. CONCLUSIONS

CIGS films grown epitaxially on GaAs by MOVPE exhibit Kirkendal voids at the CIGS/GaAs interface. The growth process results in a two-phase film with Cu_2Se segregated on the surface. Therefore, the CIGS growth is properly a solid-phase reaction between Cu_2Se and group III elements in the CIGS or dissolved in the Cu_2Se from the vapor phase. When the reaction is with atoms from the remainder of the CIGS it results in vacancies in the CIGS, primarily on the group III and group VI sublattices. These then diffuse away into the bulk of the CIGS layer. When the film is growing on a GaAs substrate the vacancies may transfer into the GaAs resulting in the Kirkendall voids and releasing Ga into the film. Because the Ga does not move rapidly, it produces a CGS layer at the substrate surface. The release of vacancies into the CIGS during the solid-phase reaction suggests that films grown by evaporation in multistage processes in which In_2Se_3 is deposited on a Cu-rich CIGS film may not result in growth of equilibrium phases. Indeed, Kirkendall voids are observed in conventional device polycrystals grown by multistage processes.[26]

The application of these materials is primarily in photovoltaic devices so a brief mention of the effects of the observed Kirkendal defects and other structures observed here on devices seems appropriate. Kirkendal voids have been observed previously in epitaxial layers and device materials and appear to have no detrimental effect on devices. Dislocations may well have a significant effect on devices but they are so rare in good device materials that they probably do not limit the actual device performances. Likewise, copper arsenides forming in the GaAs may negatively impact a heteroepitaxial device on GaAs. Even more likely to be a problem would be Cu dissolved in the GaAs, which is known to be a deep state rendering the material relatively intrinsic. Cu in the GaAs could account for series resistances in devices. Otherwise the structures observed here are unlikely to negatively impact devices. The point of this paper in regard to devices is the diffusion behavior and the formation of Kirkendal voids, both of which probably occur in device materials. These observations have implications for the growth of thin films, especially by multistep processes but are not directly tied to device performance. Finally, the second phase Cu_2Se precipitates observed here must be removed by etching before fabricating a solar cell as they would otherwise short circuit the device. These are typically removed by growth of a final In-rich layer or by etching and their occurrence is not found to damage devices if properly removed.

ACKNOWLEDGMENTS

This work was partly supported (HMI) by the German Research Ministry (BMBF) in the framework of "Hochspannungsnetz" and by the National Science Foundation under Award No. 0602938-0017756000 Materials World Network. The authors also gratefully acknowledge the support of the U.S. Department of Energy. At the beginning of the project the program "Fundamental studies of the defect chemistry of CIS" at UIUC was supported by the Office of Basic Energy Sciences under Contract No. DEFG02-91ER45439, which also supports the Center for Microanalysis of Materials at the University of Illinois. UIUC characterization of solar cell materials was also supported during the initial stage of this investigation through the National Renewable Energy Laboratory contract ADJ-2-30630-26.

[1]K. Ramanathan, *et al.* Prog. Photovoltaics **11**, 225 (2003).
[2]W. N. Shafarman, R. Klenk, and B. E. McCandless, *Proceedings of the 1996 25th IEEE Photovoltaic Specialists Conference*, May 13–17 1996, Washington, DC, (IEEE, Piscataway, NJ, 1996), p. 763–8.
[3]S. Siebentritt, Thin Solid Films **403–404**, 1 (2002).
[4]H. W. Schock *et al.*, *Proceedings of the 16th European Photovoltaic Solar Energy Conference*, edited by H. Scheer, B. McNelis, W. Palz, H. A. Ossenbrink, and P. Helm, Glasgow, (James & James, London, UK, 2000) Vol. 304.
[5]A. N. Tiwari, S. Blunier, K. Kessler, V. Zelezny, and H. Zogg, Appl. Phys. Lett. **65**, 2299 (1994).
[6]S. Niki, Y. Makita, A. Yamada, A. Obara, S. Misawa, O. Igarashi, K. Aoki, and N. Kutsuwada, ICTMC-9, 8-12 August 1993 [Jpn. J. Appl. Phys., Suppl. **32**, 161 (1993)].
[7]D. Liao and A. Rockett, J. Appl. Phys. **91**, 1978 (2002).
[8]L. C. Yang, L. J. Chou, A. Agarwal, and A. Rockett, Conference Record of the 22nd IEEE Photovoltaic Specialists Conference, Las Vegas, NV, 1991, (unpublished), p. 1185-9, Catalog No. 910H2953-8.
[9]D. J. Schroeder, G. D. Berry, and A. A. Rockett, Appl. Phys. Lett. **69**, 4068 (1996).
[10]S. Chichibu, S. Shirakata, R. Sudo, M. Uchida, Y. Harada, S. Matsumoto, H. Higuchi, and S. Isomura, *Ninth International Conference on Ternary and Multinary Compounds*, ICTMC-9, 8-12 August 1993 [Jpn. J. Appl. Phys., Suppl. **32**, 139 (1993)].
[11]M. C. Artaud-Gillet, S. Duchemin, R. Odedra, G. Orsal, N. Rega, S. Rushworth, and S. Siebentritt, J. Cryst. Growth **248**, 163 (2003).
[12]D. Liao and A. Rockett (unpublished).
[13]A. Bauknecht, S. Siebentritt, J. Albert, and M. C. Lux-Steiner, J. Appl. Phys. **89**, 4391 (2001).
[14]N. Rega, S. Siebentritt, J. Albert, and M. L. Steiner, Mater. Res. Soc. Symp. Proc. **763**, 183 (2003).
[15]Y. Tanaka, N. Akema, T. Morishita, D. Okumura, and K. Kushiya, *Proceedings of the 17th European Photovoltaic Solar Energy Conference*, Munich, Germany, edited by B. McNelis, W. Palz, H. A. Ossenbrink, and P. Helm, October 22–26, 2001, p. 989.
[16]M. Christiansen, M. Luenenbuerger, B. Schineller, M. Heuken, and H. Juergensen, Opto-Electron. Rev. **10**, 237 (2002).
[17]A. G. Cullis, N. G. Chew, and J. L. Hutchinson, *Materials Problem Solving with the Transmission Electron Microscope Symposium*, edited by L. W. Hobbs, K. K. Westmacott, and D. B.WilliamsBoston, , 1986, p. 838–8.
[18]N. G. Chew and A. G. Cullis, Ultramicroscopy **23**, 175 (1987).
[19]C. Lei, C. M. Li, A. Rockett, and I. Robertson, J. Appl. Phys., in press.
[20]C. J. Kiely, R. C. Pond, G. Kenshole, and A. Rockett, Philos. Mag. A **63**, 1249 (1991).
[21]H. Z. Xiao, L. C. Yang, and A. Rockett, J. Appl. Phys. **76**, 1503 (1994).
[22]K. Djessas, S. Yapi, G. Masse, M. Ibannain, and J. L. Gauffier, J. Appl. Phys. **95**, 4111 (2004).
[23]M. Marudachalam, H. Hichri, R. W. Birkmire, J. M. Schultz, A. B. Swartzlander, and M. M. Al-Jassim, *Proceedings of the 1996 25th IEEE Photovoltaic Specialists Conference*, May 13–17, 1996, Washington, DC, (IEEE, Piscataway, 1996), p. 805–7.
[24]D. Liao and A. Rockett, *Proceedings of the 2000 28th IEEE Photovoltiac Specialists Conference*, September 15–22, 2000, Anchorage, AK, (IEEE, Piscataway, NJ, 2000), p. 446–9.
[25]S. Siebentritt *et al.*, Sol. Energy Mater. Sol. Cells **67**, 129 (2001).
[26]C. Lei, A. Rockett, and I. Robertson, J. Appl. Phys. **100**, 073518 (2006).